Preprints, 10th IFAC International Symposium on
Advances in Automotive Control
Columbus, Ohio, USA, August 28-30, 2022

Predictive Battery Cooling in Heavy-Duty Fuel Cell Electric Vehicles

Banu Ç. Büyüker * **Alessandro Ferrara** *
Christoph Hametner **

* *Institute of Mechanics and Mechatronics, Division of Process Control and Automation, TU Wien, Vienna, Austria (e-mail: banu.bueyueker/alessandro.ferrara@tuwien.ac.at)*
** *Christian Doppler Laboratory for Innovative Control and Monitoring of Automotive Powertrain Systems, TU Wien, Vienna, Austria (e-mail: christoph.hametner@tuwien.ac.at)*

Abstract: In electric vehicles, it is essential to prevent battery overheating due to excessive ohmic losses or inadequate cooling. Indeed, the temperature of battery systems significantly impacts their performance, lifetime, and safety. This paper proposes a predictive cooling optimization method for the battery thermal management system of heavy-duty fuel cell electric vehicles. The predictive cooling strategy is based on a model predictive control (MPC) formulation to maintain the battery temperature in its optimal range (to increase efficiency) and avoid high-temperature peaks (to increase lifetime and safety). The predictive thermal management relies on the ohmic losses forecast provided by a predictive energy management system. Simulations of a real-world driving cycle validate the proposed MPC and assess the impact of the predictive horizon length, which is critical for thermal management performance. The comparison against a simple hysteresis control strategy highlights the significant benefits of the proposed MPC for higher battery efficiency and lifetime.

Keywords: Battery Thermal Management System, Fuel Cell Electric Vehicles, Model Predictive Control, Predictive Cooling Strategies, Battery Thermal Model.

1. INTRODUCTION

Transportation is one of the most significant sources of pollutants and greenhouse gas emissions. Nowadays, the automotive industry endeavors to develop clean energy vehicles like fuel cell electric vehicles (FCEVs) to reduce environmental pollution. Considering the high-power requirements of heavy-duty FCEVs, fuel cell and battery hybrid powertrains are used in these vehicles, and lithium-ion batteries are widely employed due to their relatively high energy densities and specific power capacities.

The lithium-ion batteries operate best in a specific temperature range. Outside of this range, high temperatures can lead to undesirable electrochemical behaviors on the cell structure. Therefore, developing an effective battery thermal management system (BTMS) to keep the temperature within a specified range is crucial for extending the battery life in heavy-duty FCEVs. In general, the thermal dynamics of battery systems are slow and have long time constants. Thus, developing predictive cooling strategies with long horizons can have significant benefits for increasing battery efficiency and lifetime. To this end, designing and validating the BTMS in demanding real-world driving cycles is essential.

Battery temperatures out of optimal range can accelerate battery degradation or even cause fatal disasters such as thermal runaway, battery fire, and explosion. In Wang et al. (2018), experimental investigations are held in recent years are reviewed, and the effect of battery temperature on battery degradation is shown. Passive cooling strategies to enhance heat dissipation ability are investigated. Wu et al. (2019) indicate the negative impacts of low and high temperature on battery systems. Besides restraining low and high temperatures, the importance of preventing battery temperature from having fluctuations to have a uniform temperature distribution is declared and shown. Liu et al. (2017) point out the importance of keeping Li-ion batteries within a temperature range to prevent battery performance degradation and thermal runaway.

The degradation mechanisms of the battery alter depending on various mechanical and electrochemical processes, which are affected by different operating conditions. Due to the complex cell chemistry of the batteries making a general degradation model and observing the effects of different operating conditions via a general model are rather challenging. The important point of operating conditions for this research is that high battery temperatures cause accelerated degradation due to undesired electrochemical processes. Alyakhni et al. (2021) present a battery degradation model to show the different interactions between

⋆ The financial support by the Austrian Federal Ministry for Digital and Economic Affairs and the National Foundation for Research, Technology and Development is gratefully acknowledged. This work has been created in cooperation with the Austrian research project "FC4HD" (grant no. 885044).

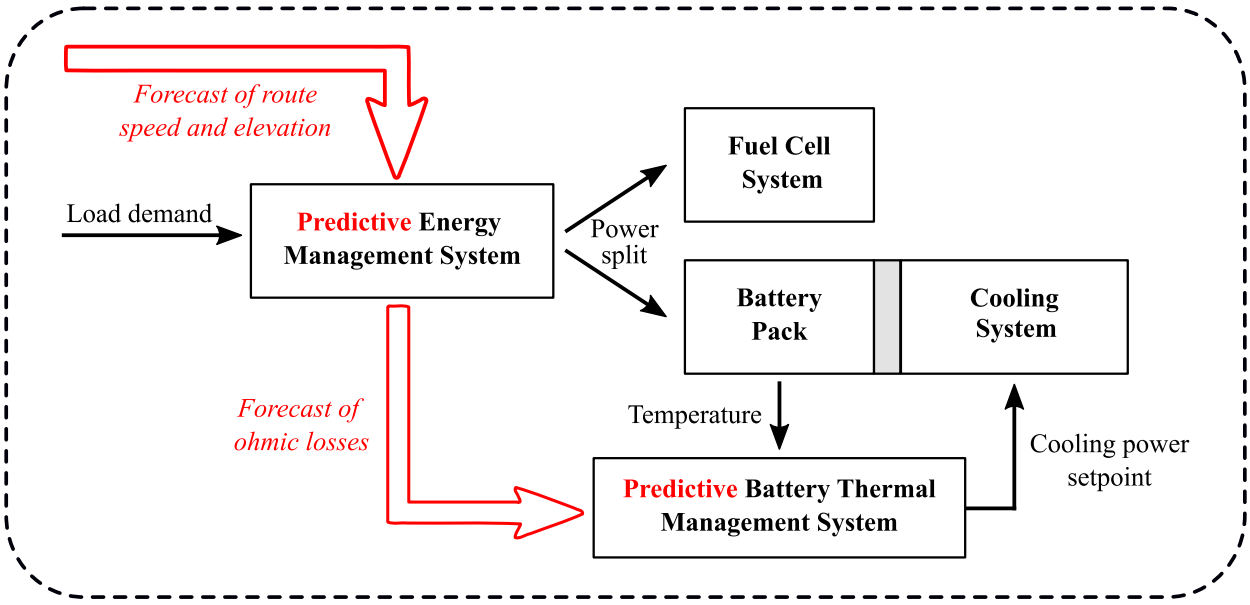

Fig. 1. Schematic representation of the interaction between predictive energy and thermal management systems based on forecasts of route speed and elevation.

battery degradation mechanisms and discuss how to avoid them with a health-conscious EMS (energy management system). In Diao et al. (2019), the tested battery cycle number vs. discharge capacity fade relation is shown for 10 °C, 25 °C, 45 °C, and 60 °C temperature values. The gradual improvement explicitly verifies the negative effect of higher temperature on degradation through 60 °C to 10 °C battery temperature. Hannan et al. (2017) indicate the optimal temperature range with the maximum life cycle as 15 °C to 45 °C for the different charge rates as 1 C, 2 C, and 3 C . Reniers et al. (2019) investigate different degradation models and the effects of operating conditions on those degradation models. Although operating conditions affect degradation differently for different battery degradation models, it is shown that accelerated degradation depends notably on high temperature.

BTMS can be categorized into three types based on different heat transfer mediums: air, liquid, and phase change material (PCM). Each system has advantages and disadvantages in terms of cost, maintenance, and effectiveness. Passive air-cooling systems are commonly used for their simplicity and electrical safety. Wang et al. (2016) states that for batteries of high energy density, an active BTMS is required, and adopting air cooling to active BTMS is complex and costly. Furthermore, an air-based cooling system can encounter temperature rise problems due to its low heat capacity and thermal conductivity. PCM has received significant attention for its potential benefits. However, Lin et al. (2021) declare that after the temperature exceeds the melting point, the cooling performance of the PCM is reduced. A liquid-based BTMS has a comparatively high transfer coefficient and thermal conductivity. Kim et al. (2019) describe the superiority of liquid cooling over air cooling. Regarding these points in the mentioned literature, this work adopts a liquid-based cooling system model.

Although the research on hardware development of BTMS is rich, the literature on the controller design is relatively poor. Rule-based controllers have been commonly employed for battery temperature regulation. For example, Zhang and Shen (2021) use a hysteresis controller for the external heating system. The hysteresis range is defined as 1 °C to avoid frequent switching, and the battery temperature is tried to keep at 15 °C. Compared to the maximum power heating and non-heating cases, the maximum driving range has been improved using the hysteresis controller for three driving cycles. However, thanks to information technology advancements, predictive control strategies can now be implemented for real-time BTMS control. Xie et al. (2020) propose a model predictive control (MPC) strategy for a radiator-based BTMS. The achievement of predictive control on reference tracking compared with an on-off controller is designated with a 60 second long predictive horizon and a 10-second long control horizon. Park and Ahn (2020) propose a stochastic MPC to obtain future heat generation for the battery cooling system by using 5 second long prediction horizons. The advantage of an MPC in comparison to an on-off controller is shown by simulation.

The literature survey revealed two main research gaps: Battery thermal management of heavy-duty fuel cell trucks and predictive cooling strategies with very long predictive horizons have not yet been investigated. The present paper fills these gaps by developing cooling strategies that can look ahead even at the entire route, which might be essential for heavy-duty FCEVs because the battery thermal dynamics are particularly slow for large components. A predictive cooling optimization method is introduced based on an MPC formulation. The MPC is utilized to exploit a real-world driving cycle forecast and use long prediction and control horizons in the control strategy. The real-world driving cycle information is used in the BTMS as an ohmic losses forecast provided by a predictive EMS for the whole driving cycle. Using long prediction and control horizons is critical to keep the battery temperature in its optimal range and avoid high-

temperature peaks. The proposed MPC is compared with a simple hysteresis controller to signify an improvement in the reference tracking of battery temperature.

The paper is structured as follows: Section 2 introduces a battery thermal model characterized by a liquid-based cooling system for the vehicle simulations and MPC derivation. Moreover, it describes the ohmic losses forecast derivation and the real-world driving cycles adopted for validating the control strategy. Section 3 defines the predictive battery cooling optimization problem and proposes a quadratic program to solve it. The system capabilities and necessary output limits are set as the constraints of the optimization problem. Full-horizon and receding-horizon MPC are implemented to evaluate the predictive horizon length requirements. Finally, Section 4 presents the optimization results and analyzes the outcomes of the different prediction horizons on the battery temperature.

2. BATTERY THERMAL MANAGEMENT SYSTEM IN HEAVY-DUTY FUEL CELL VEHICLES

Forecasts of route elevation and vehicle speed are used for predictive energy management of heavy-duty FCEVs. The resulting power split also determines a battery ohmic losses forecast, allowing for predictive thermal management. A schematic representation of such predictive control functions is depicted in Fig. 1. The EMS defines the power split of the load demand between the fuel cell and battery system. The predictive BTMS defines the cooling power setpoint for the battery cooling system based on the ohmic losses forecast coming from the predictive EMS.

This paper adopts the predictive EMS developed by Zendegan et al. (2021), which optimizes the power split considering fuel consumption and SoC (state of charge) control as optimization targets. The predictive energy management considers speed and elevation forecasts over the entire route. This feature is the main advantage compared with other predictive EMSs that use short predictive horizons (e.g., see Ferrara et al. (2021)). Indeed, due to the slow thermal dynamics of large battery systems, predictive BTMS are more effective when considering long predictive horizons and ohmic losses forecasts.

2.1 Battery Thermal Management System

Model predictive control requires a plant model to predict the future states/outputs and optimize the control input sequence. In this case, the BTMS consists of the battery system and cooling structure shown in Fig. 2, where $\dot{Q}_{loss}$ represents the heat generation due to ohmic losses and $\dot{Q}_{chill}$ cooling power absorbed by the chiller. The following linear model expresses the thermal dynamics of the BTMS:

$$C_{bat}\,\dot{T}_{bat} = \dot{Q}_{loss} - h_{bo}(T_{bat} - T_o) \tag{1a}$$
$$C_o\,\dot{T}_o = h_{bo}(T_{bat} - T_o) - h_{oc}(T_o - T_c) \tag{1b}$$
$$C_c\,\dot{T}_c = h_{oc}(T_o - T_c) - \dot{Q}_{chill} \tag{1c}$$

where T_{bat} is the battery temperature, T_o the oil one, and T_c the coolant one. Similar notation is adopted for the thermal capacities C_{bat}, C_o, and C_c. The heat exchange coefficient at the battery-oil interface is denoted with h_{bo}, and at the oil-coolant interface with h_{oc}.

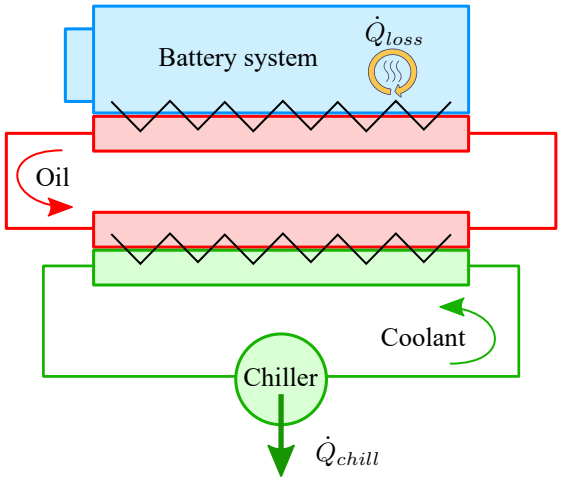

Fig. 2. Schematic of a liquid-cooled battery system.

The maximum cooling power that the chiller can provide is commonly a nonlinear function of the coolant flow, pressure, temperature, and environmental conditions. This work assumes, for simplicity, that the maximum cooling power is constant at 6 kW. The value is based on the average cooling power observed in a complex nonlinear model. The power required for the cooling system is acquired through the powertrain and added to the electrical power demand of the FCEVs.

2.2 Realistic Simulation of Heavy-Duty Fuel Cell Vehicles

The EMS of the FCEV, which is mainly necessary to calculate the electrical power demand and distribute demanded power, is summarized in Fig. 1. In a hybrid battery and fuel cell electric vehicle, EMS must be optimized with respect to driving cycles that represent driver behavior and road conditions. The simulated driving cycle in this study that includes vehicle speed, road elevation, and distance is given in Fig. 3. This driving cycle is highly demanding with 1200 m inclination, 1600 m declination, and comparatively high-speed requisition for the specified heavy-duty vehicle with 40 tons of vehicle mass. The predictive EMS architecture includes vehicle dynamics and battery and fuel cell limitations in the prediction algorithm to get effective results. The nominal battery energy and the fuel cell nominal power are configured as 53.5 kWh and 320 kW. The electrical power demand of the FCEVs is a function based on road elevation, vehicle speed, and acceleration:

$$P_{el} = f(v, \alpha, \dot{v})\ . \tag{2}$$

The detailed formulation presented in Ferrara et al. (2020) is used to realize the power splitting task shown in (3). The calculated electrical power demand of the FCEVs, P_{el} in (2) is provided by the fuel cell and the battery system:

$$P_{el} = P_{fcs} + P_{bat}. \tag{3}$$

The vehicle electrical power split between battery and fuel cell determined by the EMS are shown in Fig. 3 as P_{bat} and P_{fcs}. The calculated battery supply power, P_{bat}, is subsequently used for ohmic loss power estimations. The ohmic loss power, $\dot{Q}_{loss}$ caused by battery charging and discharging cycles is a complex electrochemical process that

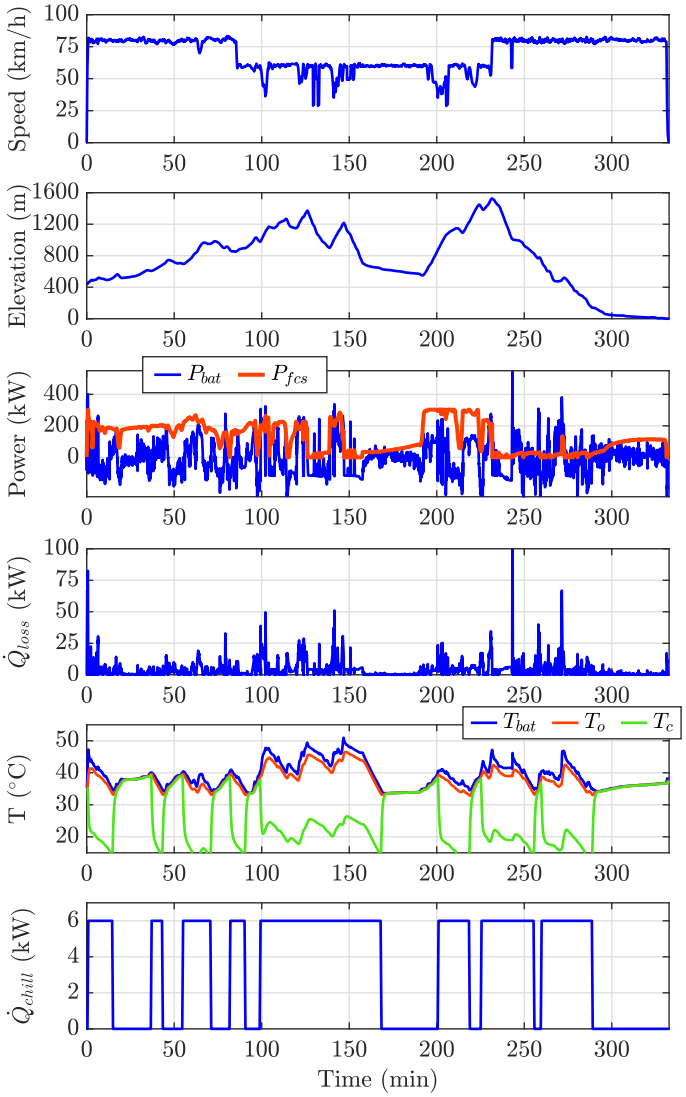

Fig. 3. Sample driving cycle, the EMS outputs and continous-time system response with hysteresis controller.

depends on the power requirement of the vehicle, current flows, and internal resistance of the battery. The battery is modeled using a simple equivalent circuit to calculate the ohmic loss. In the equivalent circuit model, the open-circuit voltage is represented with an ideal voltage source, V_{oc} connected in series with the internal resistance, R_{int}. The battery current, I_{bat}, and battery terminal voltage, V_{bat}, are included. The battery model defined in Ferrara et al. (2022) is used for the ohmic loss calculation. In accordance with the equivalent circuit model, by using Kirchoff's law, the battery current can be reformulated as:

$$I_{bat} = \frac{V_{oc} - \sqrt{V_{oc}^2 - 4P_{bat}R_{int}}}{2R_{int}}. \tag{4}$$

The ohmic losses are calculated as:

$$\dot{Q}_{loss} = R_{int}I_{bat}^2 \ . \tag{5}$$

The battery internal resistance is assumed to be constant throughout the calculations. The battery ohmic loss, $\dot{Q}_{loss}$, shown in Fig. 3 is estimated using the battery equivalent circuit model. The dependency of battery ohmic loss behavior on road elevation and vehicle speed can be obtained from the Fig. 3. It can be observed that the comparatively higher ohmic losses are observed around minutes 150 and 250 due to high elevation changes and higher acceleration and deceleration values.

Typically, rule-based hysteresis controllers are used due to their easy implementation and low computational requirements in BTMS. The threshold values of the hysteresis controller are chosen as 40 °C and 35 °C for the optimal reference tracking. The battery temperature reference is 40 °C. Fundamentally, the cooler operates at full power when the measured battery temperature is above 40 °C, and stops below 35 °C. The continuous-time system response is represented in Fig. 3 with the hysteresis controller. The battery temperature peaks around 50 °C cannot be prevented with a hysteresis controller.

3. PREDICTIVE COOLING STRATEGIES FOR BATTERY THERMAL MANAGEMENT

Predictive control algorithms are widely used for future-time information exploitation and constraint handling capabilities. In BTMS applications, predicting future temperature information and optimizing the cooling strategy according to predicted system behavior is beneficial for efficient temperature control. Nonetheless, predictive methods must provide an optimal cooling strategy by associating the real-world driving cycle data; hence the battery heat occurs depending on drivers' behavior and road conditions. In this architecture, the MPC supplies an optimal solution to the cooling problem by exploiting the battery ohmic loss forecasted through the EMS. The objective of the MPC is to predict future states in a specific prediction horizon while optimizing the control input $\dot{Q}_{chill}$ within this horizon. Besides optimizing the control input, input and output constraints are also taken into account to prevent problems that exceeding system limits can cause. In order to utilize the defined battery thermal model (1) in the MPC formulation, it is expressed as a linear state-space model,

$$\begin{aligned} \dot{x}_m &= A_m x_m + B_m u + E_m z \\ y &= C_m x_m, \end{aligned} \tag{6}$$

where $x_m = [T_{bat} \ T_o \ T_c]^T$ represent the system states, the control input is $u = \dot{Q}_{chill}$, and the disturbance is set as ohmic loss power $z = \dot{Q}_{loss}$, and the system output is taken as $y = T_{bat}$.

3.1 Discrete State-Space Model for MPC

The MPC uses the battery thermal model inside the control algorithm by employing the discrete-time system model. The system is discretized with a low sampling frequency to achieve a long prediction horizon and a low number of decision variables. Due to the low sampling time, the accuracy of the discretized model is substantial for the performance of MPC. Besides the state-space system matrices for the MPC implementation, the disturbance and control input signals described in the model should also be in discrete form. It is achieved using the zero-order hold approach for the state-space model. $\dot{Q}_{loss}$ is discretized by averaging it over the sampling time interval

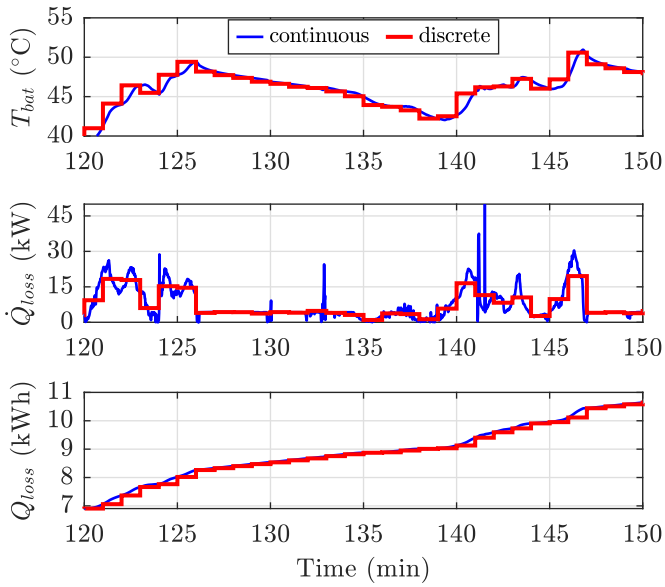

Fig. 4. Discretized system behaviour for battery temperature, battery ohmic loss power and energy.

to ensure that the ohmic loss energy Q_{loss} is preserved. In Fig. 4, the discrete-time performance of T_{bat} and $\dot{Q}_{loss}$ for 60 seconds is demonstrated. The continuous and discrete-time ohmic loss energy, Q_{loss} plots imply that the total amount of ohmic loss is kept the same after discretization.

3.2 Definition of Optimization Problem

Based on the generated battery heat forecast estimated in the EMS, see Fig. 1, a quadratic program formulation is implemented to optimize chiller power $\dot{Q}_{chill}$. This section uses the annotation given in Wang (2009) for the defined MPC problem formulation. The increment values of the discrete system states Δx_m^k and output vector y^k are augmented as new state vector for MPC implementation, $x^k = \left[\Delta x_m^k \;\; y^k\right]^T$. The augmented state-space model is presented by using the increment values of control input Δu^k and the disturbance input Δz^k:

$$\begin{aligned} x^{k+1} &= Ax^k + B\Delta u^k + E\Delta z^k \\ y^k &= Cx^k, \end{aligned} \tag{7}$$

where A, B, E, C indicate augmented state-space matrices. The augmented system output Y over prediction horizon N_p is calculated using the incremented control ΔU, and disturbance input vectors ΔZ within the prediction horizon. The compact matrix form for the prediction of the battery temperature Y can be restructured as,

$$Y = Fx^k + \Phi_U \Delta U + \Phi_Z \Delta Z, \tag{8}$$

where $F \in \mathbb{R}^{N_p \times 1}$, $\Phi_U \in \mathbb{R}^{N_p \times N_c}$ and $\Phi_Z \in \mathbb{R}^{N_p \times N_p}$ are compound matrices structured for taking the effects of the states, the control input, and the disturbance input on the output into consideration. The quadratic objective function based on the error between the battery temperature and constant temperature reference, the control input increment $\dot{Q}_{chill}$ and the slack variable s is defined as,

$$J = (Y_{ref} - Y)^T Q_y (Y_{ref} - Y) + \Delta U^T R \Delta U + s^T Q_s s, \tag{9}$$

with Q_y, Q_s positive semi-definite, and R positive definite weighting matrices of the objective function. Strictly limited output constraints can damage reference tracking performance. Furthermore, it might be impossible to find a solution in certain cases due to strict output limits. It is beneficial to set rather flexible limits to prevent these scenarios. In this problem, the strict limitation of the output variable is avoided by integrating a slack variable, s, into the optimization problem with a quadratic cost function. The control input weighting R is set to a small value because the chiller dynamics are faster than 60 seconds of sampling time, and it allows to use of the chiller power aggressively. The relation between the slack variable weighting Q_s and the output weighting Q_y is arranged as $Q_s = 100 \times Q_y$ because while integrating the soft constraints into the optimization problem, keeping the slack variable at a minimal level is important to increase the controller performance. In the defined optimization problem, the limitations for the chiller power and the optimum temperature range for the battery temperature are considered. Thus, the input and output constraints of the optimization problem are defined as follows,

$$\begin{aligned} U^{min} &\leq u^{k-1} + \Delta U \leq U^{max} \\ Y^{min} - s &\leq Y \leq Y^{max} + s. \end{aligned} \tag{10}$$

The objective function defined in (9) is minimized in order to find the optimal control input and slack variable, combined in a vector $\xi = [\Delta U \;\; s]^T$:

$$\begin{aligned} \xi^* &= \underset{\xi}{\operatorname{argmin}}\, J, \\ s.t. &: M\xi \leq \gamma. \end{aligned} \tag{11}$$

Since all constraints are linear, they can be expressed in a compact form with a matrix M and a vector γ. The MPC algorithm computes ΔU by solving optimization problem (11) via quadratic programming. The calculated ΔU is iterated to the solver after initialization, and the control input u is calculated by summation for each step.

4. OPTIMAL COOLING RESULTS

The chiller power $\dot{Q}_{chill}$ is obtained by solving the defined optimization problem of the battery cooling system in Section 3.2 and fed into continuous-time battery model (6) to realize the battery cooling system simulations. The simulation results are acquired for both full and receding prediction horizon optimization approaches, and the setpoint for the output, T_{bat}, is taken as constant 40 °C in all solutions. The prediction and control horizons are set equal, $N_p = N_c$ in all scenarios, and only referred to N_p for simplicity.

4.1 Full Horizon Optimization

The full-horizon optimization is realized in this study to observe maximum improvement in reference tracking that could be achieved with the MPC. The full horizon optimization computes the chiller power $\dot{Q}_{chill}$ through the whole trajectory of heavy-duty FCEV by minimizing the cost function (9). The prediction horizon N_p is set to the full length of the driving cycle to reach a full horizon optimal solution. The full-horizon optimization of

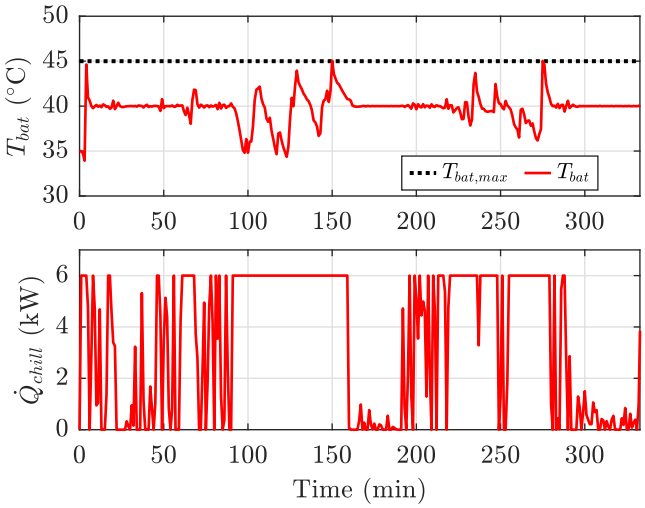

Fig. 5. Full-horizon MPC results for the battery temperature and cooling power.

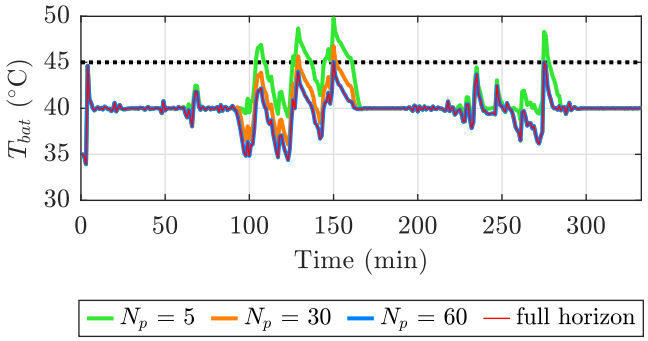

Fig. 6. The battery temperature results for 5, 30, 60 minutes, and full-horizon prediction horizons.

the quadratic equations such as (11) could require long computational time for long trajectories. Thanks to discretization with a 60 seconds sampling time implemented in Section 3.1, the full-horizon optimization of the defined problem is realized in 3 seconds. All simulations are carried out on a standard office computer with the AMD Ryzen™ 7 PRO 5850U CPU and 32 GB of RAM. The results of the full-prediction horizon MPC are presented in Fig. 5. A significant improvement in reference tracking is succeeded with predictive cooling compared to the hysteresis controller shown in Fig. 3. This plot also shows the characteristics of the control input and the 6 kW input limit.

4.2 Receding Horizon Optimization

The receding horizon optimization provides an optimal solution for a relatively short time in the future, N_p, and aims at the online implementation of MPC in real-time applications. It minimizes the objective function (11) iteratively to compute the control strategy within N_p. The prediction horizon N_p is increased gradually, and the battery temperature is observed for each entity to observe the effects of different prediction horizons on the controller performance, t_{comp}. Due to 60 seconds sampling time, to acquire, for instance, a 20 minutes prediction horizon, N_p is set to 20 steps. In Fig. 6, the characteristic of the system output T_{bat} is depicted for various prediction horizons. The better reference tracking performance is achieved by

Table 1. The effect of prediction horizon on the battery temperature peaks.

N_p	5	10	20	40	60	80	FH
T_{bat}^{max} (°C)	49.7	48.9	46.7	46.1	45.0	45.0	45.0
t_{comp} (s)	0.2	0.3	1.1.	6.60	14.9	29.7	3.3

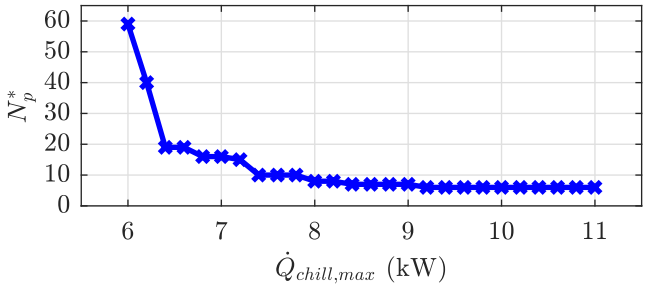

Fig. 7. The prediction horizon sensitivity to maximum cooling power limit.

increasing the prediction horizon. Also, with the increase in prediction horizon, the improvement in preventing the peaks of battery temperature can be seen explicitly. The 45 °C maximum battery temperature limit is satisfied with 60 steps of prediction horizon and full-horizon cases. Nevertheless, it could be observed that from the green and orange lines in Fig. 6 MPC allows deviations outside of limits with the help of the slack variable. In the cases of a constraint violation, the optimization problem can not find any solution without the slack variable.

Table 1 indicates the maximum battery temperature peaks and recorded computational times t_{comp} for the whole driving cycle with different prediction horizons. The noticeable effect of the prediction horizon on preventing battery temperature peaks can be seen in this table. Since the computational complexity of the MPC algorithm highly depends on the prediction horizon, while deciding the prediction horizon for the defined optimization problem, the required computational time should also be considered. Nevertheless, even 29.7 seconds of the highest recorded computational time is adequate because the real-time factor calculated by fractioning the computation time to the driving cycle duration is $1.5 \times 10^{-3} \ll 1$. The lower computational time obtained with the full horizon is due to one loop of optimization for the whole trajectory. Both Table 1 and Fig. 6 shows that after 60 minutes of prediction horizon the battery temperature response stays similar. As a result, it is concluded that 60 minutes of prediction horizon could be applied for this particular optimization problem.

The effect of the prediction horizon on system performance could also be used for deciding the chiller power requirement. By analyzing the prediction horizon - chiller power relation given in Fig. 7 considering the chiller power capability of the system, an effective prediction horizon can be guessed. Furthermore, unnecessary cooling power enlargement can be avoided using the same method depending on the prediction horizon choice. For this purpose, in Fig. 7, the minimum number of required prediction horizon steps to stay below 45 °C maximum battery temperature limit is presented with respect to ascending maximum chiller

power limits $\dot{Q}_{chill}$. It is observed that with the increment of the maximum power capability of the chiller, the required prediction horizon N_p^* decreases exponentially. It can be concluded that 8 kW of chiller power is sufficient for this specific battery cooling system; hence after 8 kW of chiller power, N_p^* nearly stabilizes.

5. CONCLUSION

The work described in this paper shows that a good reference tracking of the battery temperature can be achieved by using the proposed predictive cooling strategy in a BTMS. By investigating the impact of the prediction horizon on the battery temperature, it is concluded that high efficiency in cooling performance can be attained with an appropriately chosen horizon length.

The investigation of desired prediction horizon for altering maximum cooling power constraints shows that by increasing the maximum cooling power limit, the required prediction horizon for keeping battery temperature at the optimal range could be decreased. Also, this method can help to decide the feasible prediction horizon according to the available power capacity of the cooling system.

The battery cooling has been significantly improved with the proposed predictive strategy compared to the hysteresis controller based on a real-world driving cycle. Furthermore, it is expected that such a strategy helps limit the battery accelerated degradation by avoiding temperature peaks that cause unwanted chemical reactions.

However, to compensate for the uncertainties caused by the driver's behavior, the future work would be the evaluation of the uncertainty compensation capability of the controller regarding various driving cycles forecasted into BTMS with EMS, and the controller can be modified for uncertainty compensation.

REFERENCES

Alyakhni, A., Boulon, L., Vinassa, J.M., and Briat, O. (2021). A comprehensive review on energy management strategies for electric vehicles considering degradation using aging models. *IEEE Access*, 9, 143922–143940. doi:10.1109/ACCESS.2021.3120563.

Diao, W., Saxena, S., Han, B., and Pecht, M. (2019). Algorithm to determine the knee point on capacity fade curves of lithium-ion cells. *Energies*, 12(15). doi: 10.3390/en12152910.

Ferrara, A., Jakubek, S., and Hametner, C. (2021). Energy management of heavy-duty fuel cell vehicles in real-world driving scenarios: Robust design of strategies to maximize the hydrogen economy and system lifetime. *Energy Conversion and Management*, 232, 113795. doi: https://doi.org/10.1016/j.enconman.2020.113795.

Ferrara, A., Okoli, M., Jakubek, S., and Hametner, C. (2020). Energy management of heavy-duty fuel cell electric vehicles: Model predictive control for fuel consumption and lifetime optimization. volume 53, 14205–14210. Elsevier B.V. doi:10.1016/j.ifacol.2020.12.1053.

Ferrara, A., Zendegan, S., Koegeler, H.M., Gopi, S., Huber, M., Pell, J., and Hametner, C. (2022). Optimal calibration of an adaptive and predictive energy management strategy for fuel cell electric trucks. *Energies*, 15(7). doi:10.3390/en15072394.

Hannan, M., Lipu, M., Hussain, A., and Mohamed, A. (2017). A review of lithium-ion battery state of charge estimation and management system in electric vehicle applications: Challenges and recommendations. *Renewable and Sustainable Energy Reviews*, 78, 834–854. doi: https://doi.org/10.1016/j.rser.2017.05.001.

Kim, J., Oh, J., and Lee, H. (2019). Review on battery thermal management system for electric vehicles. doi: 10.1016/j.applthermaleng.2018.12.020.

Lin, J., Liu, X., Li, S., Zhang, C., and Yang, S. (2021). A review on recent progress, challenges and perspective of battery thermal management system. doi: 10.1016/j.ijheatmasstransfer.2020.120834.

Liu, H., Wei, Z., He, W., and Zhao, J. (2017). Thermal issues about li-ion batteries and recent progress in battery thermal management systems: A review. doi: 10.1016/j.enconman.2017.08.016.

Park, S. and Ahn, C. (2020). Computationally efficient stochastic model predictive controller for battery thermal management of electric vehicle. *IEEE Transactions on Vehicular Technology*, 69, 8407–8419. doi: 10.1109/TVT.2020.2999939.

Reniers, J.M., Mulder, G., and Howey, D.A. (2019). Review and performance comparison of mechanical-chemical degradation models for lithium-ion batteries. *Journal of The Electrochemical Society*, 166(14), A3189–A3200. doi:10.1149/2.0281914jes.

Wang, L. (2009). *Model Predictive Control System Design and Implementation Using MATLAB*. Springer Publishing Company, Incorporated, 1st edition.

Wang, Q., Jiang, B., Li, B., and Yan, Y. (2016). A critical review of thermal management models and solutions of lithium-ion batteries for the development of pure electric vehicles. doi:10.1016/j.rser.2016.05.033.

Wang, Y., Gao, Q., Wang, G., Lu, P., Zhao, M., and Bao, W. (2018). A review on research status and key technologies of battery thermal management and its enhanced safety. doi:10.1002/er.4158.

Wu, W., Wang, S., Wu, W., Chen, K., Hong, S., and Lai, Y. (2019). A critical review of battery thermal performance and liquid based battery thermal management. *Energy Conversion and Management*, 182, 262–281. doi: 10.1016/j.enconman.2018.12.051.

Xie, Y., Wang, C., Hu, X., Lin, X., Zhang, Y., and Li, W. (2020). An mpc-based control strategy for electric vehicle battery cooling considering energy saving and battery lifespan. *IEEE Transactions on Vehicular Technology*, 69, 14657–14673. doi:10.1109/TVT.2020.3032989.

Zendegan, S., Ferrara, A., Jakubek, S., and Hametner, C. (2021). Predictive battery state of charge reference generation using basic route information for optimal energy management of heavy-duty fuel cell vehicles. *IEEE Transactions on Vehicular Technology*, 70(12), 12517–12528. doi:10.1109/TVT.2021.3121129.

Zhang, S. and Shen, W. (2021). Rule-based control of battery external heating for electric vehicle during driving at low temperatures. *IEEE ACCESS*, 9, 149360–149371. doi:10.1109/ACCESS.2021.3124786.